Rare Metal Materials and Engineering
Volume 55, Issue 5, May 2026
Available online at www.rmme.ac.cn

Science Press

Cite this article as: Chen Gongyu, Cheng Li, Liu Zihan, et al. Design and Phase-Field Simulation of Core-Shell Microstructure in TiNb Binary Alloy[J]. Rare Metal Materials and Engineering, 2026, 55(05): 1129-1136.
DOI: https://doi.org/10.12442/j.issn.1002-185X.20250225.

ARTICLE

Design and Phase-Field Simulation of Core-Shell Microstructure in TiNb Binary Alloy

Chen Gongyu[1], Cheng Li[1], Liu Zihan[1], Zhang Gang[3], Zhu Jiaming[1,2,4]

[1] Shenzhen Research Institute of Shandong University, Shenzhen 518057, China; [2] School of Civil Engineering, Shandong University, Jinan 250061, China; [3] School of Physics and Opto-Electronic Technology, Baoji University of Arts and Sciences, Baoji 721016, China; [4] Institute of Materials Intelligent Technology, Liaoning Academy of Materials, Shenyang 110004, China

Abstract: The core-shell structure in bulk TiNb binary alloy was designed and studied by phase-field simulations, where various core-shell structures were obtained by precise control of the initial and boundary conditions of the TiNb binary alloy system during spinodal decomposition, and then the formation mechanism of core-shell structure was revealed. In addition, the influences of initial temperature gradient, average temperature, and initial concentration distribution of the system on the core-shell structure were investigated. Results show that the initial concentration gradient is the key factor for forming the core-shell structure. Besides, larger initial temperature gradient and higher average temperature can promote the formation of core-shell structure, which can be stabilized by adjusting the initial concentration distribution of the Nb-rich region in TiNb binary alloy. As a theoretical basis, this research provides a novel and simple strategy for the preparation of TiNb-based alloys and other materials with peculiar core-shell structures and desirable mechanical and physical properties.

Key words: TiNb binary alloy; phase-field simulation; spinodal decomposition; core-shell structure; microstructure evolution

1 Introduction

With the advancement of science and technology, material microstructure plays a more and more important role in determining the mechanical properties[1–5]. Recent studies demonstrate that the core-shell structures in materials can significantly enhance the material performance[6–8]. For example, Ti-based alloys with the core-shell structure, fabricated from plasma-sintered Ti-N particles, present exceptional yield strength (about 1.4 GPa) and thermal stability (exceeding 1100 ℃, which is 71% of the melting temperature), rivaling nanostructured materials[9]. The harder Ti-N shell ensures high strength, whereas the softer Ti core contributes to the plasticity (fracture plasticity of about 12%). In addition to the application for mechanical properties, core-shell structures are widely adopted in the nanoscale active materials[10], catalysts, electronics, photoluminescence, and biomedicine[11]. For instance, in carbon dioxide conversion, core-shell structured catalysts address several key challenges, such as sintering and activity loss during CO_2 reforming, insufficient selectivity in thermocatalytic hydrogenation, and low efficiency in photocatalytic/electrocatalytic processes[12]. However, current methods struggle to the production of bulk materials with uniform core-shell structures.

As an efficient and cost-effective approach, spinodal decomposition can be used to achieve nanoscale concentration modulation in materials, such as ferrochromium[13–14], titanium-based alloys[15–22], manganese-copper[23], aluminum-based alloys[24], and polymer materials[25–27]. Such concentration modulation markedly improves the strength and plasticity of materials[15–18]. Besides, the spinodal decomposition is also employed to produce and predict the core-shell structure in various material systems[28–32]. However, the controllable core-shell structure has seldom been achieved by simple design and

Received date: May 29, 2025
Foundation item: National Natural Science Foundation of China (12372152); Guangdong Basic and Applied Basic Research Foundation (2023A1515011819, 2024A1515012469); Shandong Provincial Natural Science Foundation (ZR2023MA058)
Corresponding author: Zhu Jiaming, Ph. D., Professor, Shenzhen Research Institute of Shandong University, Shenzhen 518057, P. R. China, E-mail: zhujiaming@sdu.edu.cn; Zhang Gang, Ph. D., Associate Professor, School of Physics and Opto-Electronic Technology, Baoji University of Arts and Sciences, Baoji 721016, P. R. China, E-mail: gzhang20@163.com

modification of the initial and boundary conditions of the material system with the miscibility gap.

In this research, multilayer core-shell-structured bulk materials were prepared via a phase-field model[33–39] by precisely controlling the initial and boundary conditions of the TiNb binary alloy system under spinodal decomposition, providing a novel and simple strategy for the preparation of bulk materials with core-shell structures.

2 Establishment of Phase-Field Model

2.1 Formulation of Gibbs free energy

According to thermodynamics[40], Landau's phase transition theory[41], and gradient thermodynamics[42–43], the total free energy of an inhomogeneous system can be obtained by Eq.(1):

$$F = \int_V \left[f_{ch} + \frac{1}{2}\kappa(\nabla c)^2 \right] \mathrm{d}V \quad (1)$$

where V is volume; f_{ch} is the local chemical free energy density per unit volume; κ is the gradient energy coefficient (1.15×10^{-10} J/m); other parameters are explained in Ref. [44–48]. Based on the regular solution approximation[44], the local chemical free energy density f_{ch} of TiNb binary alloy can be given by Eq.(2), as follows:

$$f_{ch} = cG^{\beta}_{Nb} + (1-c)G^{\beta}_{Ti} + RT\left[c\ln c + (1-c)\times\ln(1-c)\right] + c(1-c)L^{\beta}_{TiNb} \quad (2)$$

where c is the atom fraction of Nb element; R is the gas constant of 8.314 J·(mol·K)$^{-1}$; T is the absolute temperature (400 K in this research); L^{β}_{TiNb} is the binary interaction parameter of 13 045.3 J·mol^{-1}; other parameters are explained in Ref.[47–48].

In this case, G^{β}_{Nb} and G^{β}_{Ti} can be expressed by Eq.(3–4)[47–48], respectively:

$$G^{\beta}_{Nb} = -8519.353 + 142.045475T - 26.4711T\ln T + 0.203475\times10^{-3}T^2 - 0.350119\times10^{-6}T^3 + 93399T^{-1} \quad (298.15\ \mathrm{K} < T < 2750\ \mathrm{K}) \quad (3)$$

$$G^{\beta}_{Ti} = -1272.064 + 134.71418T - 25.5768T\ln T - 0.663845\times10^{-3}T^2 - 0.278803\times10^{-6}T^3 + 7208T^{-1} \quad (298.15\ \mathrm{K} < T < 1155\ \mathrm{K}) \quad (4)$$

2.2 Governing equation of spinodal decomposition

The temporal evolution of microstructure is controlled by the nonlinear Cahn-Hilliard-Cook diffusion equation[45–46], as follows:

$$\frac{\partial c(\boldsymbol{r},t)}{\partial t} = \nabla\cdot\left[M(c)\cdot\nabla\left(\frac{\delta F}{\delta c}\right)\right] + \xi(\boldsymbol{r},t) \quad (5)$$

where t is time; $c(\boldsymbol{r},t)$ is the atom fraction of Nb element; $M(c)$ denotes the mobility; F is the total free energy; ξ is the Langevin noise term for the thermal fluctuation; other parameters are explained in Ref. [45–46]. In this study, it is assumed that the mobility $M(c)$ is a constant for simplicity, i. e., $M(c)=M=1$ in this research. In addition, the variate derivative in Eq. (5) can be expressed as $\partial f_{ch}/\partial c - \kappa\nabla^2 c$. Thus, Eq.(3) can be expressed as follows:

$$\frac{\partial c(\boldsymbol{r},t)}{\partial t} = M\nabla^2\left[\frac{\partial f_{ch}}{\partial c} - \kappa\nabla^2 c\right] + \xi(\boldsymbol{r},t) \quad (6)$$

Eq. (6) can be solved numerically by the finite-difference method.

2.3 Initial condition of spinodal decomposition

In this research, a model possessing centrosymmetry was proposed, where a Nb-rich spherical region is contained in a cube, as shown in Fig. 1a. To reduce computational

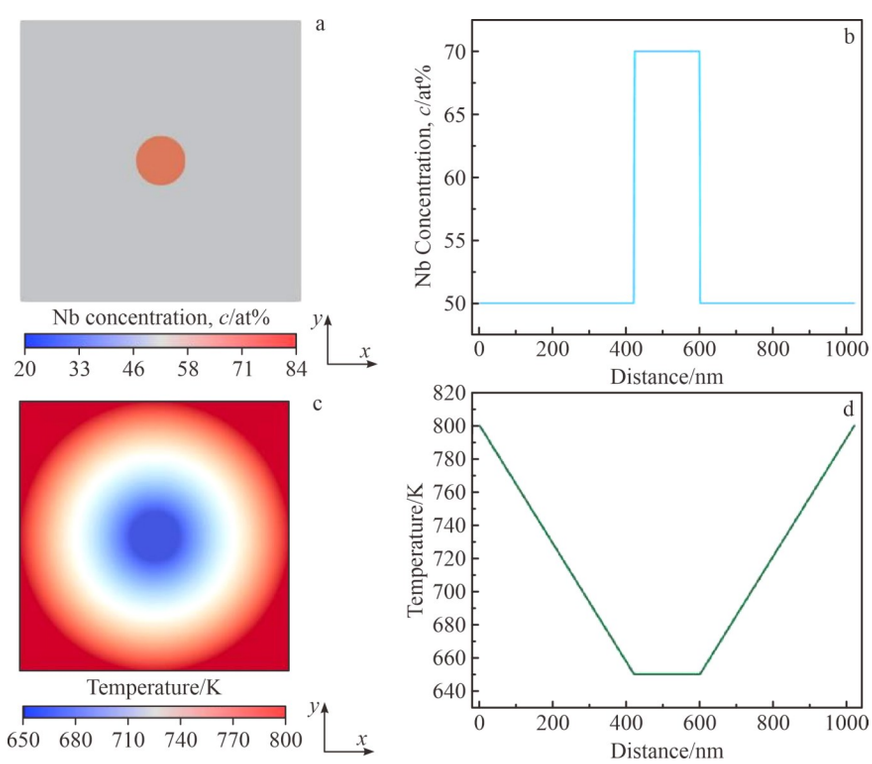

Fig.1 Initial Nb concentration (a) and temperature (c) conditions for phase-field simulation; Nb concentration (b) and temperature (d) profiles along x-axis passing through the center of the circle in Fig.1a and Fig.1c, respectively

complexity, a two-dimensional system with length of 1024 nm in each dimension was employed. Periodic boundary conditions were applied along both x and y directions. The model features a circular Nb-rich region in the system center with a radial temperature gradient established along the radius direction (Fig. 1c). The Nb concentration and temperature profiles along the x-axis passing through the circle centers are shown in Fig.1b and 1d, respectively.

3 Simulation Results

Fig. 2 shows the microstructure evolution of spinodal decomposition under temperature gradient of 650–800 K with Nb-rich particles concentrated in the central region. t^* indicates the dimensionless time, which is defined as $t^*=Mt/l^2$ with l as the length of simulation cell. The decomposition rate significantly varies with temperature, and the decomposition phenomenon occurs predominantly in the lower-temperature regions (Fig.2b). With the aging proceeding, a multilayer core-shell structure develops towards the outside around the Nb-rich core (Fig. 2c – 2e). However, this structure is unstable. During the subsequent coarsening process, the central core-shell region gradually merges with adjacent areas (Fig.2f–2h). The obtained core-shell structure is different from that from the previous results, where most core-shell structures are single-layer, and the controlling process of core-shell structure formation is rather complex for practical applications[28–32].

4 Discussion

4.1 Mechanisms of core-shell structure formation

Fig. 3a illustrates the formation process of the first ring layer of core-shell structure. Due to the centrosymmetry of the model, only Nb concentration and driving force profiles along the x-axis are presented for analysis. The Nb concentration profiles in Fig.3d reveal that when the sharp central interface diffuses outward, an inner Nb-lean zone, an adjacent Nb-rich zone, and an outer Nb-lean zone simultaneously form. The outermost Nb-lean zone has the Nb reduction of 3.5×10^{-7} mol (red region in Fig. 3e), and the annular Nb-rich zone has the Nb increase of 1.1×10^{-6} mol (blue region in Fig. 3e). It is found that the outer depletion alone cannot account for the enrichment of ring. Thus, the inner Nb-rich ring supplies Nb to both the central region and the first-layer ring region. Fig. 3b presents the chemical free energy density curve of TiNb alloy at 650 K. For clarity, Fig.3c displays the difference between chemical free energy density and corresponding data from red tangent line in Fig. 3b, which reveals that the chemical free energy primarily exists between two points corresponding to the maximum and inflection points marked by the red dashed line. In this system, spinodal decomposition may cause a decrease in Nb concentration in high-Nb-content regions and an increase in Nb concentration in low-Nb-content regions, as indicated by the blue dashed line in Fig.3c. This process may result in higher energy compared with that at the pre-decomposition state. Conversely, if the Nb concentration increases in high-Nb-content regions and decreases in low-Nb-content regions, as indicated by black dashed line in Fig.3c, the system energy becomes lower. This analysis demonstrates that based on the structure in this research, the number of Nb-rich regions will further increase, but the number of Nb-lean regions will decrease.

Fig. 4 demonstrates that the initial Nb concentration gradient creates a sustained driving force around the Nb-rich region, maintaining positive/negative values during the prolonged period. Consequently, the peripheral region evolves

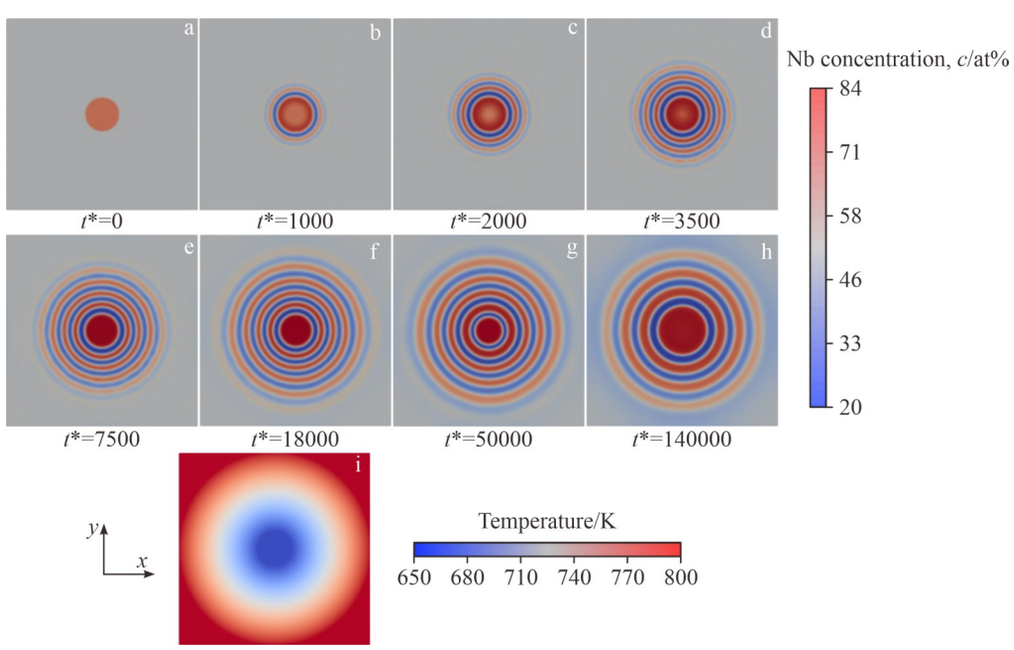

Fig.2 Microstructure evolution of spinodal decomposition in TiNb binary alloy with a Nb-rich (70at% Nb) region at center under temperature gradient of 650–800 K: (a) t^*=0, (b) t^*=1000, (c) t^*=2000, (d) t^*=3500, (e) t^*=7500, (f) t^*=18 000, (g) t^*=50 000, and (h) t^*=140 000; temperature distribution of phase-field model of TiNb binary alloy with 70at% Nb under temperature gradient of 650–800 K (i)

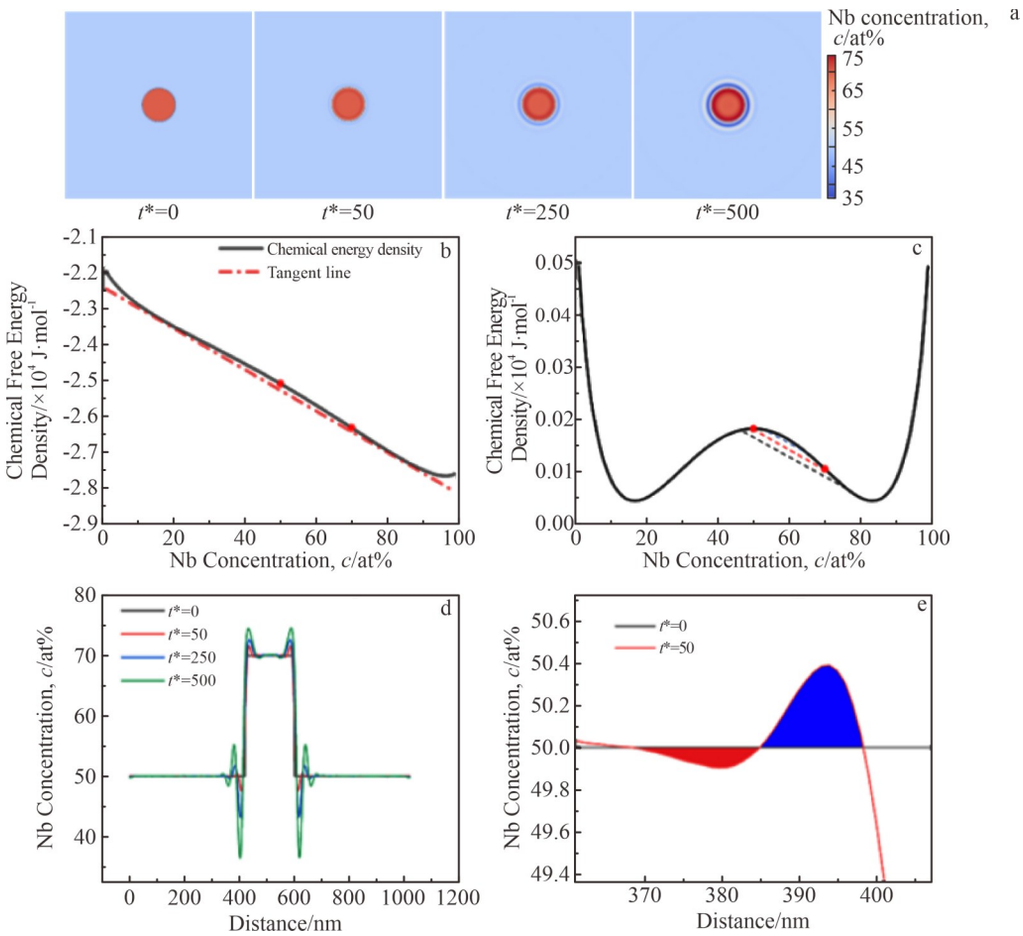

Fig.3 Schematic diagrams of formation process of the first layer of core-shell structure (a); chemical free energy density of TiNb alloy at 650 K (b); difference between chemical free energy density and corresponding data from red tangent line in Fig. 3b (c); Nb concentration profiles at different t^* conditions (d); localized enlargement of Nb concentration profiles at t^*=0 and t^*=50 (e)

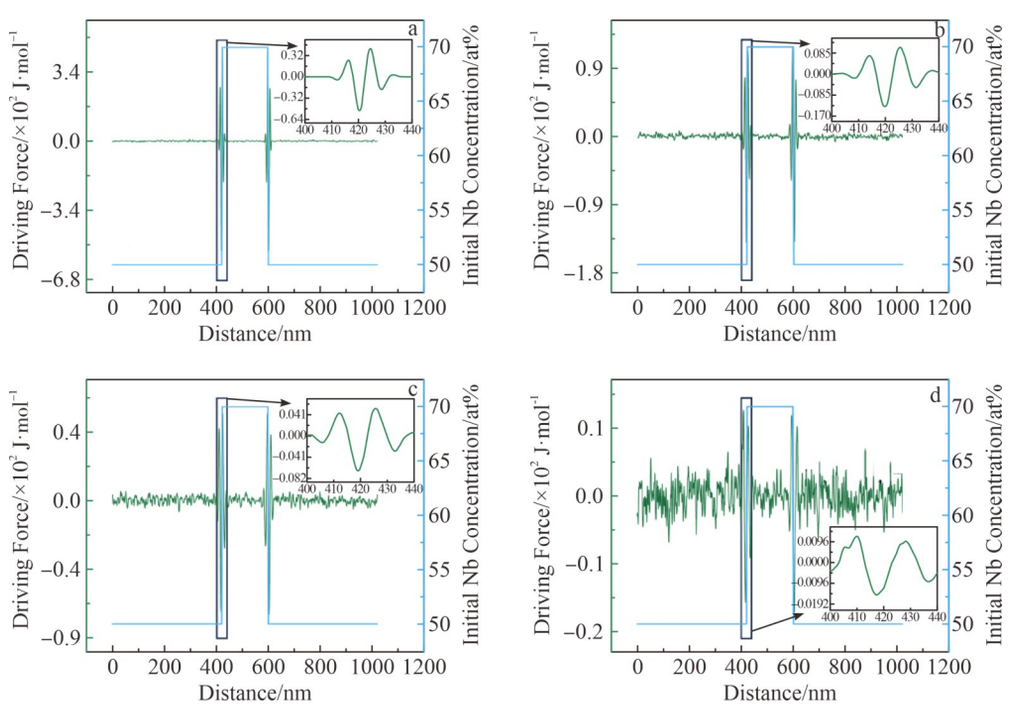

Fig.4 Variations of driving force of spinodal decomposition under different t^* conditions for TiNb binary alloys containing Nb-rich (70at% Nb) region with temperature gradient of 650–800 K passing through the circle center along x-axis: (a) t^*=0.01; (b) t^*=1; (c) t^*=2; (d) t^*=9

first, forming the core-shell structure, as shown in Fig.3a.

The formation mechanism of the multilayer core-shell structure can be explained through its influence on neighboring regions. As shown in Fig. 2b – 2e, the initially formed core-shell structure remains stable until the coarsening phenomenon occurs. This stable structure serves as a boundary condition for the adjacent region, inducing their evolution towards a new equilibrium. This propagating influence is defined as the induced effect in this research.

The temperature-dependent evolution kinetics plays a crucial role in the formation of multilayer core-shell structure. Fig. 5 reveals that the chemical potential shows greater sensitivity to composition changes at lower temperatures, i.e., the lower the region temperature, the faster the evolution speed. The temperature gradient causes a decrease in evolution speed with the increase in distance from the model center. Consequently, when one region completes its core-shell formation, the adjacent region remains at the early stage of spinodal decomposition. In this research, it is assumed that decomposition does not simultaneously occur in the neighboring regions.

During the formation of multilayer core-shell structure, the Nb concentration gradient of established core-shell structure replicates the initial gradient, thereby inducing new core-shell formation in the adjacent regions. This chain-like reaction propagates outward, ultimately generating the complete bulk core-shell structure. This induced sequence explains the formation of multilayer core-shell structure. The formation mechanism of the multilayer core-shell structure in this research is different from that in other researches, though both of them are intimately correlated with the spinodal decomposition process[28–32]. Besides, the strategy of producing and controlling the core-shell structure by adjusting the initial and boundary conditions of the bulk system in this research is more convenient and simpler in practical application.

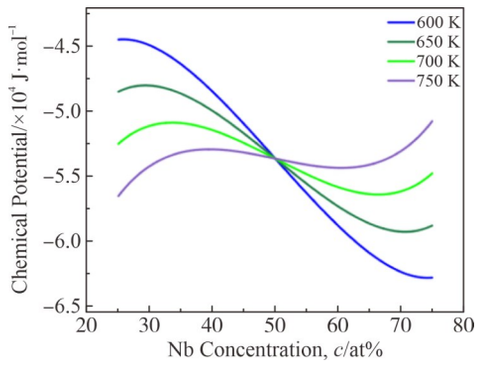

Fig.5 Chemical potentials of TiNb binary alloy at different temperatures

The formation of core-shell structure fundamentally depends on the initial Nb concentration gradient, whereas the development of the structure is primarily governed by spatial variations of evolution speed, which is influenced by 3 key factors: temperature gradient magnitude, average temperature, and initial composition.

4.2 Effect of temperature gradient on formation of core-shell structure

The formation of bulk core-shell structures critically depends on the spatial variation of evolution speed induced by the temperature gradient. The speed variation is directly related to the magnitude of the temperature gradient.

Fig. 6 demonstrates the microstructure evolution under the reduced temperature gradient (650 – 700 K). As shown in

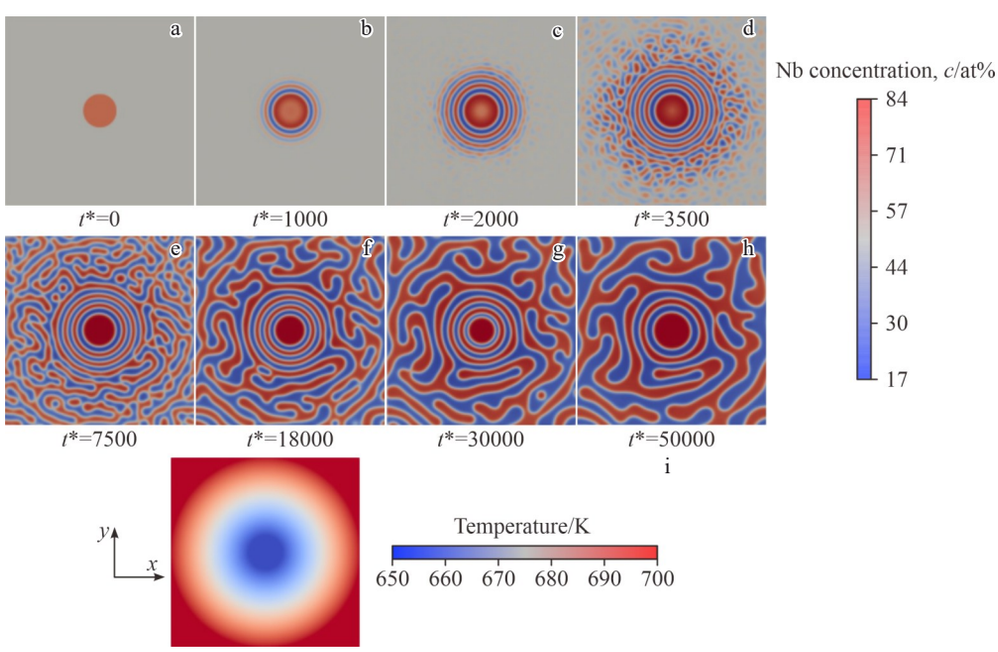

Fig.6 Microstructure evolution of spinodal decomposition in TiNb binary alloy with a Nb-rich (70at% Nb) region at center under temperature gradient of 650–700 K: (a) t^*=0, (b) t^*=1000, (c) t^*=2000, (d) t^*=3500, (e) t^*=7500, (f) t^*=18 000, (g) t^*=30 000, and (h) t^*=50 000; temperature distribution of phase-field model of TiNb binary alloy with 70at% Nb under temperature gradient of 650–700 K (i)

Fig.6a–6c, the central Nb-rich region first evolves into a core-shell structure during the early stage of decomposition. However, with the evolution proceeding, the edge regions with Nb-lean/rich zone form (Fig. 6f), the interpenetrated structures develop (Fig. 6e), and ultimately the dissolution of central core-shell structure occurs during the coarsening stage (Fig.6f–6h).

These phenomena stem from the reduced speed difference between central and edge regions caused by the smaller temperature gradient. Comparative analysis of Fig. 6d and Fig.2d indicates that the evolution of the edge region is faster with temperature gradient of 650 – 800 K. The accelerated evolution of the edge region leads to the formation of an interpenetrated structure before the core-shell boundary condition is established. Ultimately, the system develops a homogeneous interpenetrated structure during the coarsening process (Fig.6f–6h), demonstrating that a sufficient magnitude of temperature gradient is essential for bulk core-shell structure formation.

4.3 Effect of average temperature on formation of core-shell structure

The formation of multilayer core-shell structures is governed by spinodal decomposition kinetics, which is directly influenced by the average temperature of the system. This can be clearly demonstrated by Fig. 7, which shows the microstructure evolution of TiNb alloys at reduced average temperatures (573 – 723 K). The morphology development during the early stage of decomposition is similar to that under temperature gradient of 650 – 700 K, i. e., spinodal decomposition begins at the low-temperature central region and then the core-shell structure forms (Fig.7a–7b). However, during the intermediate and later stages, with the fixed temperature gradient (ΔT=150 K) and the temperature gradient same as that in Fig. 2, the edge region develops an interpenetrated structure rather than the expected shell structure. This structural discrepancy results from accelerated decomposition kinetics at lower average temperatures. The increased decomposition rate gives rise to the premature formation of Nb-lean/rich regions in the edge region before establishing the necessary boundary conditions for shell development, ultimately leading to the formation of an interpenetrated structure. These observations demonstrate that the formation of bulk core-shell structure is hindered to a certain extent when the average temperature falls below a critical threshold.

4.4 Effect of initial content of Nb-rich region on core-shell structure

Owing to the lower temperature, the central regions in the model (Fig. 2a, Fig. 6a, and Fig. 7a) first undergo spinodal decomposition and then enter the coarsening stage. This process leads to the gradual absorption of smaller central particles by larger edge-region particles, resulting in the gradual merger of the central region with adjacent layers of the core-shell structure. Therefore, stabilizing the bulk core-shell structure needs to delay the onset of the coarsening process.

Fig. 8 presents the microstructure evolution of spinodal decomposition in TiNb binary alloy with a Nb-rich (55at% Nb) region at center under temperature gradient of 650 – 800 K. Similar to previous cases, spinodal decomposition is preferentially initiated in the low-temperature central region and then forms a core-shell structure (Fig. 8b). However, unlike the TiNb binary alloy with 70at% Nb in Fig.2, the TiNb binary alloy with 55at% Nb exhibits slower disappearance of

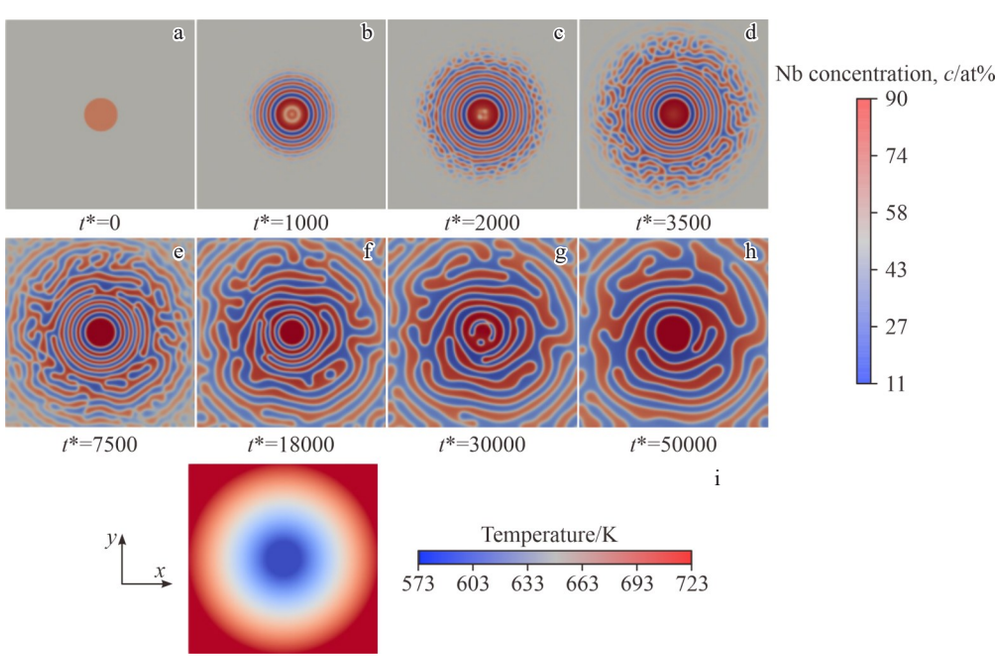

Fig.7 Microstructure evolution of spinodal decomposition in TiNb binary alloy with a Nb-rich (70at% Nb) region at center under temperature gradient of 573–723 K: (a) t^*=0, (b) t^*=1000, (c) t^*=2000, (d) t^*=3500, (e) t^*=7500, (f) t^*=18 000, (g) t^*=30 000, and (h) t^*=50 000; temperature distribution of phase-field model of TiNb binary alloy with 70at% Nb under temperature gradient of 573–723 K (i)

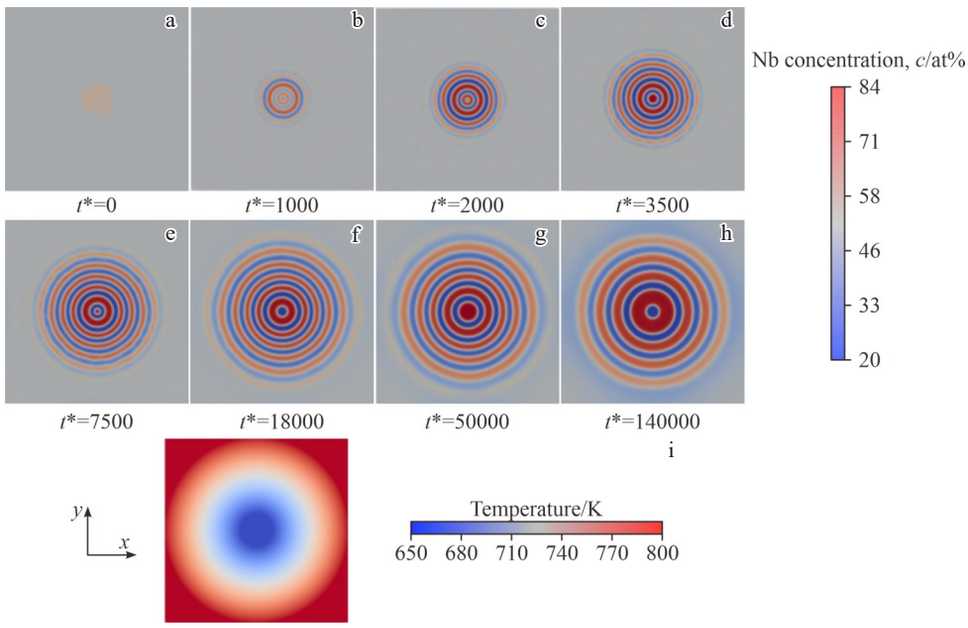

Fig.8 Microstructure evolution of spinodal decomposition in TiNb binary alloy with a Nb-rich (55at% Nb) region at center under temperature gradient of 650–800 K: (a) t^*=0, (b) t^*=1000, (c) t^*=2000, (d) t^*=3500, (e) t^*=7500, (f) t^*=18 000, (g) t^*=50 000, and (h) t^*=140 000; temperature distribution of phase-field model of TiNb binary alloy with 55at% Nb under temperature gradient of 650–800 K (i)

the central core-shell structure while simultaneously developing extended shell structures through induced effects (Fig. 8c – 8f). These observations demonstrate that the initial composition of the Nb-rich region critically determines when the central region enters the coarsening stage. This phenomenon arises because the Nb concentration in the central region for the TiNb binary alloy with 55at% Nb is farther from the equilibrium concentration (about 84at% Nb), compared with that of the TiNb binary alloy with 70at% Nb, causing a later reaching of equilibrium central region and consequently delaying the entry into the coarsening stage. The induced effect of the initial concentration gradient further promotes the formation of a new core-shell structure in the TiNb binary alloy with 55at% Nb (Fig. 8c – 8f), which is inhibited in the TiNb binary alloy with 70at% Nb by insufficient available Ti particles for shell formation due to higher Nb content. During the coarsening process, the small-sized secondary core-shell structure is preferentially absorbed by surrounding larger particles (Fig. 8f – 8g), which enhances the stability of the primary central structure. This sequential process ultimately yields the well-defined bulk core-shell structure (Fig.8h).

5 Conclusions

1) A novel strategy for producing bulk core-shell structures by controlling the initial and boundary conditions of spinodal decomposition is proposed. The initial concentration gradient is the primary factor driving the formation of core-shell structures.

2) The temperature gradient of the system leads to a gradual decrease in speed of spinodal decomposition from the central region to the outside region. Larger temperature gradients and higher average temperatures promote the formation of bulk core-shell structures.

3) The bulk core-shell structure can be stabilized by adjusting the initial composition of the Nb-rich region.

References

1 Cheng Z, Zhou H F, Lu Q H *et al*. *Science*[J], 2018, 362(6414): 559
2 Du R, Song H, Gao F *et al*. *International Journal of Plasticity*[J], 2023, 170: 103743
3 Peng Q, Liu X M, Wei Y G. *Journal of the Mechanics and Physics of Solids*[J], 2021, 156: 104604
4 Hu J, Song H, Sandfeld S *et al*. *Tribology International*[J], 2022, 173: 107660
5 Peng Q, Ye X, Wu H *et al*. *Mechanism and Machine Theory*[J], 2020, 154: 104034
6 Wan Xinyu, Zhao Dong, Xiang Ling *et al*. *Rare Metal Materials and Engineering*[J], 2023, 52(12): 4155 (in Chinese)
7 Wang Y L, Kang Y T, Zhang W J *et al*. *Rare Metal Materials and Engineering*[J], 2024, 53(12): 3348
8 Luo J J, Quan C W, Zhang J J *et al*. *Rare Metal Materials and Engineering*[J], 2024, 53(11): 3053
9 Zhang Y S, Zhao Y H, Zhang W *et al*. *Scientific Reports*[J], 2017, 7: 40039
10 Ma X, Li Y, Hussain I *et al*. *Advanced Materials*[J], 2020, 32: 2001291
11 Mao G Y, Yang W J, Bu F X *et al*. *Journal of Materials Chemistry B*[J], 2014, 2: 4481
12 Das S, Pérez-Ramírez J, Gong J *et al*. *Chemical Society Reviews* [J], 2020, 49: 2937
13 Li Y S, Li S X, Zhang T Y. *Journal of Nuclear Materials*[J], 2009, 395: 120
14 Findik F. *Materials & Design*[J], 2012, 42: 131
15 Zhu J M, Wang D, Gao Y P *et al*. *Materials Today*[J], 2020,

33: 17
16 Zhu J M, Gao Y P, Wang D *et al*. *Materials Horizons*[J], 2019, 6: 515
17 Zhu J M, Wu H H, Yang X S *et al*. *Acta Materialia*[J], 2019, 181: 99
18 Zhu J M, Gao Y P, Wang D *et al*. *Acta Materialia*[J], 2017, 130: 196
19 Ishiguro Y, Tsukada Y, Koyama T. *Computational Materials Science*[J], 2020, 174: 109471
20 Su Y, Liang C, Sun X *et al*. *Acta Materialia*[J], 2023, 246: 118697
21 Hao Y L, Wang H L, Li T *et al*. *Journal of Materials Science & Technology*[J], 2016, 32: 705
22 Wang H L, Hao Y L, He S Y *et al*. *Scripta Materialia*[J], 2017, 133: 70
23 Tsuchiya K, Sato H, Edo S *et al*. *Materials Science and Engineering A*[J], 1999, 273–275: 181
24 Shen K, Yin Z M, Wang T. *Materials Science and Engineering A* [J], 2008, 477: 395
25 Zhang G, Qin Z Y, Qian Y *et al*. *Computational Materials Science*[J], 2022, 213: 111659
26 Zhang G, Yang T, Yang S *et al*. *Physical Review E*[J], 2017, 96: 032501
27 Zhang G, Qiao G J. *Journal of Chemical Physics*[J], 2013, 139: 134903
28 Peng Y L, Wang N. *Journal of Materials Science & Technology* [J], 2020, 38: 64
29 Li Y C, Shi R P, Wang C P *et al*. *Physical Review E*[J], 2011, 83: 041502
30 Wang C P, Liu X J, Shi R P *et al*. *Applied Physics Letters*[J], 2007, 91: 141904
31 Hsiao C L, Magnusson R, Palisaitis J *et al*. *Nano Letters*[J], 2015, 15(1): 294
32 Seppanen T, Persson P O A, Hultman L *et al*. *Journal of Applied Physics*[J], 2005, 97: 083503
33 Zhao Y H. *npj Computational Materials*[J], 2023, 9: 94
34 Hao Mengyuan, Li Pei, Wang Dong. *Materials China*[J], 2022, 41(7): 497 (in Chinese)
35 Xin T Z, Tang S, Ji F *et al*. *Acta Materialia*[J], 2022, 239: 118248
36 Chen L Q, Zhao Y H. *Progress in Materials Science*[J], 2022, 124: 100868
37 Sun Qiming, Shen Wenlong, Liao Yuxuan *et al*. *Rare Metal Materials and Engineering*[J], 2025, 54(3): 671 (in Chinese)
38 Zhu Wei, Cheng Dazhao, Liu Caiyan *et al*. *Rare Metal Materials and Engineering*[J], 2024, 53(8): 2193 (in Chinese)
39 Zhu J M, Wu H, Wu Y *et al*. *Acta Materialia*[J], 2021, 207: 116665
40 Gibbs J W. *Transactions*[J], 1876, 3: 108
41 Wannier G H. *Statistical Physics*[M]. New York: John Wiley and Sons, Inc., 1966
42 Cahn J W. *Journal of Chemical Physics*[J], 1965, 42(1): 93
43 Cahn J W, Hilliard J E. *Journal of Chemical Physics*[J], 1958, 28(2): 258
44 Binder K, Fratzl P, Kostorz G. *Phase Transformations in Materials*[M]. Weinheim: Wiley VCH, 2001: 409
45 Cahn J W. *Acta Metallurgica*[J], 1961, 9(9): 795
46 Chen L Q. *Annual Review of Materials Research*[J], 2002, 32: 113
47 Dinsdale A T. *Calphad*[J], 1991, 15(3): 317
48 Tokunaga T, Matsumoto S, Ohtani H *et al*. *Materials Transactions*[J], 2007, 48(2): 89

TiNb二元合金中核壳结构的设计及相场模拟

陈恭昱[1]，程　利[1]，刘子晗[1]，张　刚[3]，朱家明[1,2,4]

(1. 山东大学深圳研究院，广东 深圳 518057)

(2. 山东大学 土建与水利学院，山东 济南 250061)

(3. 宝鸡文理学院 物理与光电技术学院，陕西 宝鸡 721016)

(4. 辽宁材料实验室 材料智能技术研究所，辽宁 沈阳 110004)

摘　要：采用相场模拟对块体TiNb二元合金中的核-壳结构进行了设计和研究，通过精确控制TiNb合金体系中调幅分解过程的初始和边界条件，以获得不同的核-壳结构，并揭示了核-壳结构的形成机理。此外，研究了体系初始温度梯度、平均温度和初始浓度分布对核-壳结构的影响。结果表明，初始浓度梯度是形成核-壳结构的关键因素。此外，较大的初始温度梯度和较高的平均温度能促使核-壳结构的形成，并可通过调节TiNb合金中富铌区的初始浓度分布来稳定核-壳结构。作为理论基础，本研究为制备具有特殊核-壳结构和理想力学与物理性能的TiNb基合金以及其它材料提供了一种新颖且简单的策略。

关键词：TiNb二元合金；相场模拟；调幅分解；核壳结构；微观组织演化

作者简介：陈恭昱，男，1999年生，硕士，山东大学深圳研究院，广东 深圳 518057，E-mail：gzhang20@163.com